

Supplementary Information

Methods

MSV fabrication and characterization:

In brief, heavily doped P-type silicon wafers were porosified by electrochemical etching using electrical current in HF ethanoic solution. Afterwards, low-temperature oxide (LTO) sacrificial layer was deposited on the wafer followed by patterning cylindrical trenches. To release the resulting MSV from LTO, the silicon wafers were sonicated in IPA solution for 1 min. MSV were then dried and oxidized in a piranha solution [1:2 H₂O₂: H₂SO₄ (v/v)] at 100–110°C for 2 h, thoroughly washed and stored at 4°C in water. Volumetric MSV size, size distribution and count were measured using a Multisizer 4 Coulter Particle Counter (Beckman Coulter, Fullerton, CA, USA). Zeta potential was assessed using a Zetasizer nano ZS (Malvern Instruments, Malvern, Worcestershire, UK) by measuring particle suspension containing at least 2×10^5 particles in phosphate buffer (PB, pH 7.4) in a Zetasizer capillary cell.

Labeling RBC and macrophages for intravital microscopy

Three days before imaging, autologous red blood cells (RBC) were collected from mice by drawing 50–100 µL of blood from orbital sinus to EDTA-coated microcentrifuge tube. Blood was centrifuged at 270 rcf for 10 minutes, and the serum layer was discarded without disrupting the RBC pellet. RBCs were then transferred to a fresh uncoated tube and incubated with 7.5 µL DiO marker in 750 µL PBS solution at 37°C for 15 minutes. After removal of leftover DiO and washing twice by centrifugation (150 rcf, 5 minutes), RBCs were resuspended in 100 µL sterile PBS and injected back into the mice intravenously as previously reported¹. Three days later, the remnants of labelled RBCs were taken up by macrophages and the blue DiO marker was used to track macrophages accessible from the circulation.

Tumor sphere generation

For tumor sphere formation, methods we have previously published were used². Briefly, 4T1 cells were treated with 50µl of Nanoshuttle™, trypsinized, counted and seeded on 96-well low attachment plate at a seeding density of 15000 cells/mL. 100µL of cell suspension was pipetted to the wells and the 96-well magnetic spheroid drive was kept under the plates to ensure the sphere formation. Spheres were formed after the first day and were ready to be used in experiments after 2 days of culture.

Measurement of sphere growth in cell culture

The spheroid growth kinetics were measured by microscopy image analysis of sphere diameter increase as well as sphere area over the course of the experiments. **Supp Fig 2** illustrates the growth of the untreated control. The cells formed tight spheres within the first 6 hours of seeding, and the growth remained constant within the first 5 days. The experiments were initiated within the second to third day after cell seeding.

Mathematical model of tumor response to MSV- nAb-PTX

We provide a brief overview of previous work modeling the potential role of macrophages in cancer therapy. In early work, Owen and Sherratt^{3,4} presented mathematical models to evaluate the effects of macrophage presence, influx, and ability to selectively kill tumor cells in avascular tumors. Subsequent modeling evaluated the ability of macrophages engineered to target tumor cells⁵ or deliver drug⁶, finding that such approaches are non-intuitively sensitive to tumor and therapy parameters. These concepts were further developed in⁷, showing that effective targeting of hypoxic tumor cells by macrophages would benefit from limited-diffusivity or non-cell-cycle dependent drugs. In⁸, Owen et al. developed a model to explore the efficacy and timing of therapy with drug-delivering macrophages pre-loaded with magnetic nanoparticles, finding that the combination of conventional and macrophage-based therapies could be synergistic. Recently, a mathematical model was presented to explore the role of tumor macrophage hypoxia inducible factors (HIFs) in chemotherapy effectiveness⁹.

We next describe the mathematical model to simulate the effect of therapy with MSV-nAb-PTX loaded macrophages to treat breast cancer metastases to the liver.

1. Tumor growth

The tumor model component is based on Macklin et al.¹⁰. Briefly, the tumor tissue is denoted by Ω and its boundary by Σ . In general, tumor tissue may have a proliferating region Ω_P (typically in the order of 100-200 μm) in which cells have sufficient oxygen and nutrients, a hypoxic region Ω_H in which oxygen and nutrients are sufficient for survival but not for proliferation, and a necrotic region Ω_N in which oxygen and nutrients are insufficient for survival. The tumor growth velocity (non-dimensionalized) is implemented via a generalized Darcy's law¹⁰:

$$\mathbf{v}_c = -\mu\nabla P + \chi_E \nabla E \quad [\text{Equation 1}]$$

where μ is cell-mobility representing the net effects of cell-cell and cell-matrix adhesion, P is oncotic pressure, χ_E is haptotaxis, and E is ECM density. Definitions for χ_E and E are in¹⁰. By assuming that the cell density is constant in the proliferating region, the overall tumor growth is associated with the rate of volume change:

$$\nabla \cdot \mathbf{v}_c = \lambda_p \quad [\text{Equation 2}]$$

where λ_p is non-dimensional net proliferation rate (see below). Here, the cell density is assumed not to exceed 70% of the total tissue, with the remainder composed of extracellular matrix.

2. Angiogenesis

The angiogenesis model component simulates the model by McDougall et al.¹¹ and is based on Macklin et al. and Wu et al.^{10,12}, representing blood flow, vascular leakage and vascular network remodeling due to wall shear stress and mechanical stresses imposed by the tumor tissue. The angiogenesis model is described in detail by Macklin et al. and Wu et al.^{10,12}. We simulate a simplified liver vascular organization composed of square elements, acknowledging that in biological reality these elements are heterogeneously delineated by the sinusoids between the portal tracts and central veins at high density. As the tumor grows within this vascular environment, the tissue may experience heterogeneous access to elements diffusing from the vasculature, which may depend on tissue pressure as well as distance from the nearest vascular source.

3. Transport of oxygen

Oxygen σ is simulated to be transported from the location of the vasculature, supplied at rates λ_{neo}^σ and λ_{pre}^σ from the neo- and pre-existing vasculature, respectively, diffuse with a coefficient D_σ , taken up both by normal cells (with a rate λ_{tissue}^σ) and tumor cells (λ_{tumor}^σ in the proliferating region and q_σ in the hypoxic region), and decay (with rate λ_V^σ) in the necrotic regions. The formulation is ¹⁰:

$$0 = \nabla \mathbf{q}(D_\sigma \nabla \sigma) - \lambda^\sigma(\sigma)\sigma + \lambda_{ev}^\sigma(\mathbf{x}, t, \mathbf{1}_{vessel}, p, \sigma, h) \quad [\text{Equation 3}]$$

$$\lambda^\sigma = \begin{cases} \lambda_{tissue}^\sigma & \text{outside } \Omega \\ \lambda_{tumor}^\sigma & \text{in } \Omega_P \\ q_\sigma(\sigma) & \text{in } \Omega_H \\ \lambda_N^\sigma & \text{in } \Omega_N \end{cases} \quad [\text{Equation 4}]$$

where \mathbf{x} is position in space, t is time, $\mathbf{1}_{vessel}$ is the characteristic function for vasculature (equals 1 at vessel locations and 0 otherwise), p is the tumor (solid) pressure, and h is the hematocrit in the vascular network related to oxygen extravasation (following ¹⁰). The extravasation is modulated by the extravascular interstitial pressure p_i scaled by the effective pressure p_e , with k_{p_i} being the weight of the convective transport component of small molecules ¹³:

$$\lambda_{ev}^\sigma = \bar{\lambda}_{ev}^\sigma \mathbf{1}_{vessel}(\mathbf{x}, t) \left(\frac{h}{\bar{H}_D} - \bar{h}_{min} \right)^+ \left(1 - k_{p_i} \frac{p_i}{p_e} \right) (1 - \sigma) \quad [\text{Equation 5}]$$

where $\bar{\lambda}_{ev}^\sigma$ is the constant transfer rate from both pre-existing and tumor-induced vessels. Constants \bar{H}_D and \bar{h}_{min} respectively represent normal and minimum blood hematocrit required for oxygen extravasation.

4. Transport of drug

Macrophages are modeled to extravasate as point sources of drug from the vasculature in proportion to the local concentration of macrophage chemoattractants (e.g., pro-angiogenic factors), and to preferentially migrate towards tissue regions (e.g., hypoxic tissue) along the increasing gradient of these chemoattractants. The transport of drug s is simulated at the location ($\mathbf{1}_{macrophage}$) of each macrophage:

$$0 = \nabla \mathbf{q}(D_s \nabla s) - \lambda^s(s)s + \lambda_{ev}^s(\mathbf{x}, t, \mathbf{1}_{macrophage}, p, s, h) \quad [\text{Equation 6}]$$

The drug release is described as:

$$\lambda_{ev}^s = \bar{\lambda}_{ev}^s \mathbf{1}_{macrophage}(\mathbf{x}, t) \left(\frac{C^t}{C_s} - s \right) \quad [\text{Equation 7}]$$

where $\bar{\lambda}_{ev}^s$ is the constant transfer rate of drug from the macrophage. The drug level in the MSVs carried by the macrophages is initially \bar{C}_s ; in time the release is assumed to be of the form $C^t = \bar{C}_s e^{-\alpha t}$, where the decay α is estimated experimentally ¹³. This assumes first order kinetics, for which the release is concentration dependent.

The boundary conditions for all the diffusion equations are $\frac{\partial B}{\partial n} = 0$ (zero Neumann condition).

5. Drug effect on the tumor

The drug is assumed effective only where it reaches a concentration above a threshold T_{drug} , and then it only affects proliferating cells to simulate the cell-cycle dependent effect of Paclitaxel. For simplicity, cell death is assumed to be an instantaneous process. The drug effect is included into the proliferation term λ_p , where $\bar{\lambda}_{effect}$ is a rescaling factor with units of effect per drug concentration, and \bar{C}_s rescales the drug concentration s in the tissue¹³:

$$\lambda_p = \begin{cases} 0 & \text{outside } \Omega \\ s(1 - \bar{\lambda}_{effect} \bar{C}_s s) \mathbf{1}_{s > T_{drug}} - \lambda_{\Lambda} & \text{in } \Omega_P \\ 0 & \text{in } \Omega_H \\ -G_N & \text{in } \Omega_N \end{cases} \quad [\text{Equation 8}]$$

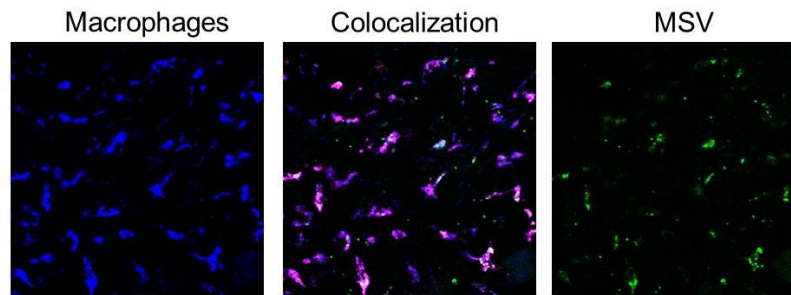
where λ_{Λ} is the natural apoptosis rate and G_N is the non-dimensional rate of volume loss in the necrotic regions assuming that cellular debris is constantly degraded and fluid is removed.

The main parameters of the model and their values are described in **Supp. Table 1**.

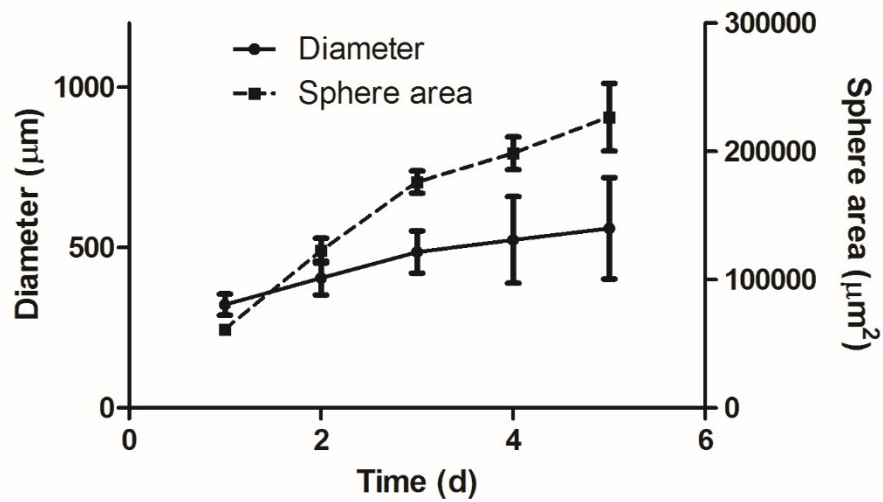
Parameter	Value	Reference
Tumor proliferation rate	1 day ⁻¹	Measured <i>in vitro</i>
Tumor tissue threshold for hypoxia	0.5750	Calibrated to match 3D cell culture
Tumor tissue threshold for necrosis	0.5325	Calibrated to match 3D cell culture
Oxygen diffusivity	1 (*)	¹²
Oxygen transfer rate from vasculature	5 (*)	¹²
Oxygen uptake rate by proliferating tumor cells	1.5 (*)	¹²
Oxygen uptake rate by hypoxic tumor cells	1.3 (*)	¹²
Oxygen uptake rate by tumor microenvironment	0.12 (*)	¹²
Oxygen decay rate	0.35 (*)	¹²
ABX transfer rate from vasculature or MSV-nab-PTX macrophages	5 (*)	¹³
ABX diffusivity	0.25 (*)	Estimated from experimental data
ABX uptake rate by proliferating tumor cells	1.5 (*)	¹³
ABX decay rate	20 hr. half-life	¹⁴
MSV per MSV-nab-PTX macrophage	10	Measured <i>in vitro</i>
ABX per MSV	0.0015 ng	Measured <i>in vitro</i>
Paclitaxel per ABX molecule	10%	¹⁴
ABX <i>in vitro</i> EC50 (48 hrs.) for 4T1 cells (monolayer)	125 ng/mL	Measured <i>in vitro</i>
Percentage of macrophages per tumor lesion total cells	10%	Measured <i>in vitro</i>
Resistance differential between monolayer and 3D cell culture when macrophages are present	1	Measured <i>in vitro</i>
Number of macrophages needed <i>in vivo</i> to attain EC50 <i>in vitro</i>	27,778 / mm ³	Calculated from experimental data
ABX murine dose <i>in vivo</i>	75 mg/kg	Measured <i>in vivo</i>

Supplementary Table 1. Main computational model parameters and associated values. (*) Value is rescaled by the square of the simulation system characteristic length (1 cm) and divided by the system characteristic time (1 sec) multiplied by the oxygen diffusivity ¹⁵ (1 x 10⁻⁵ cm² s⁻¹).

Figures



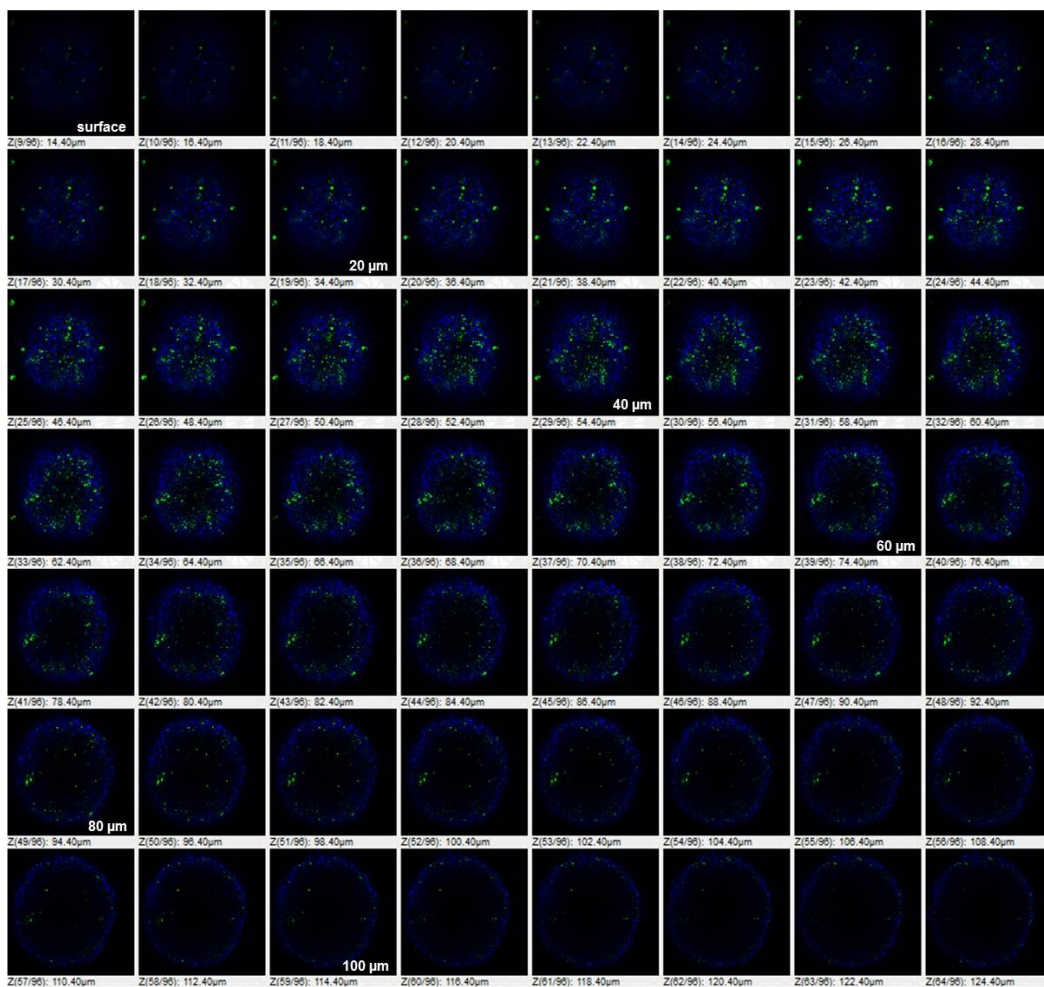
Supplementary figure 1. Disposition of FITC-labelled MSV (green) in the mouse liver. Macrophages (blue) were labeled via DiO labelling of autologous RBC, which were scavenged by macrophages after 3 d (methods in supplementary). Colocalization of MSV in macrophages can be detected as purple signal.



Supplementary Figure 2. Characteristics of 4T1 sphere growth in diameter and sphere area when seeded in density of 1500 cells/well

a

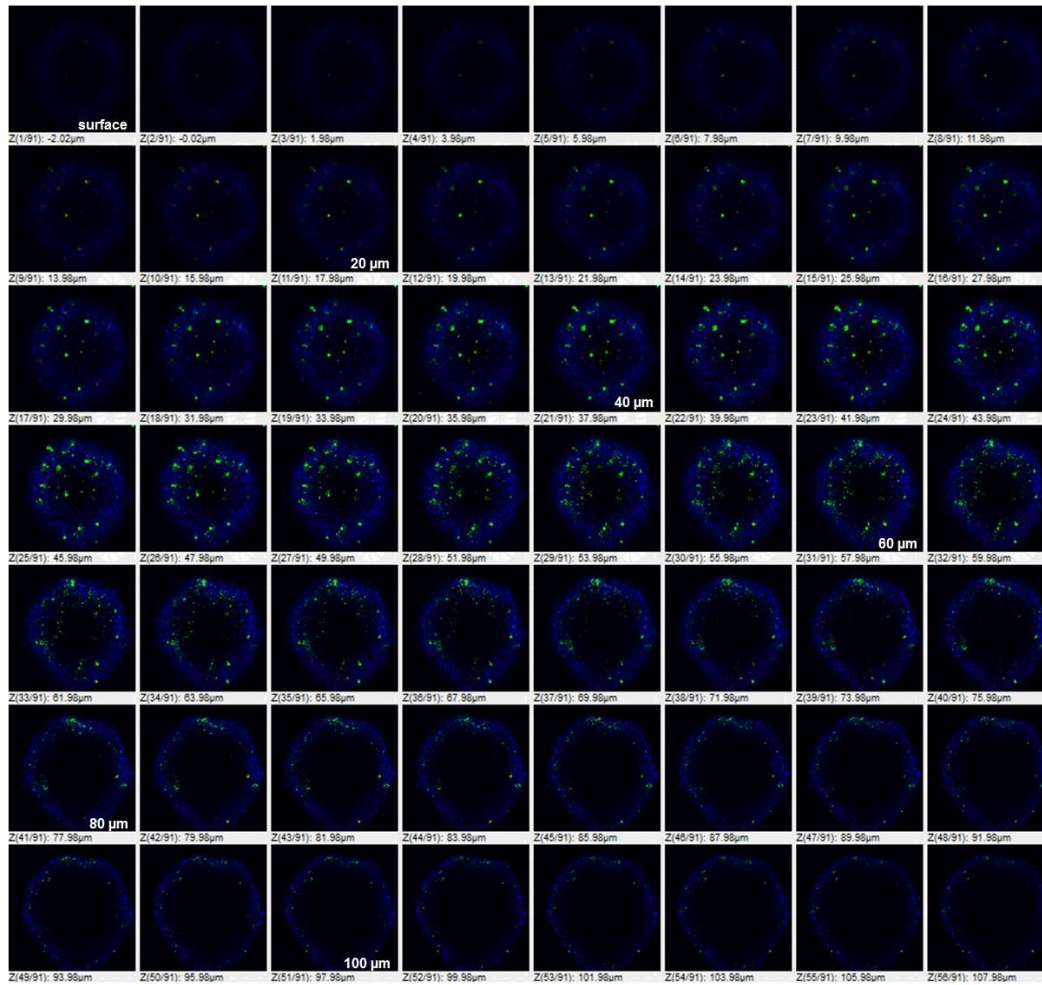
Control



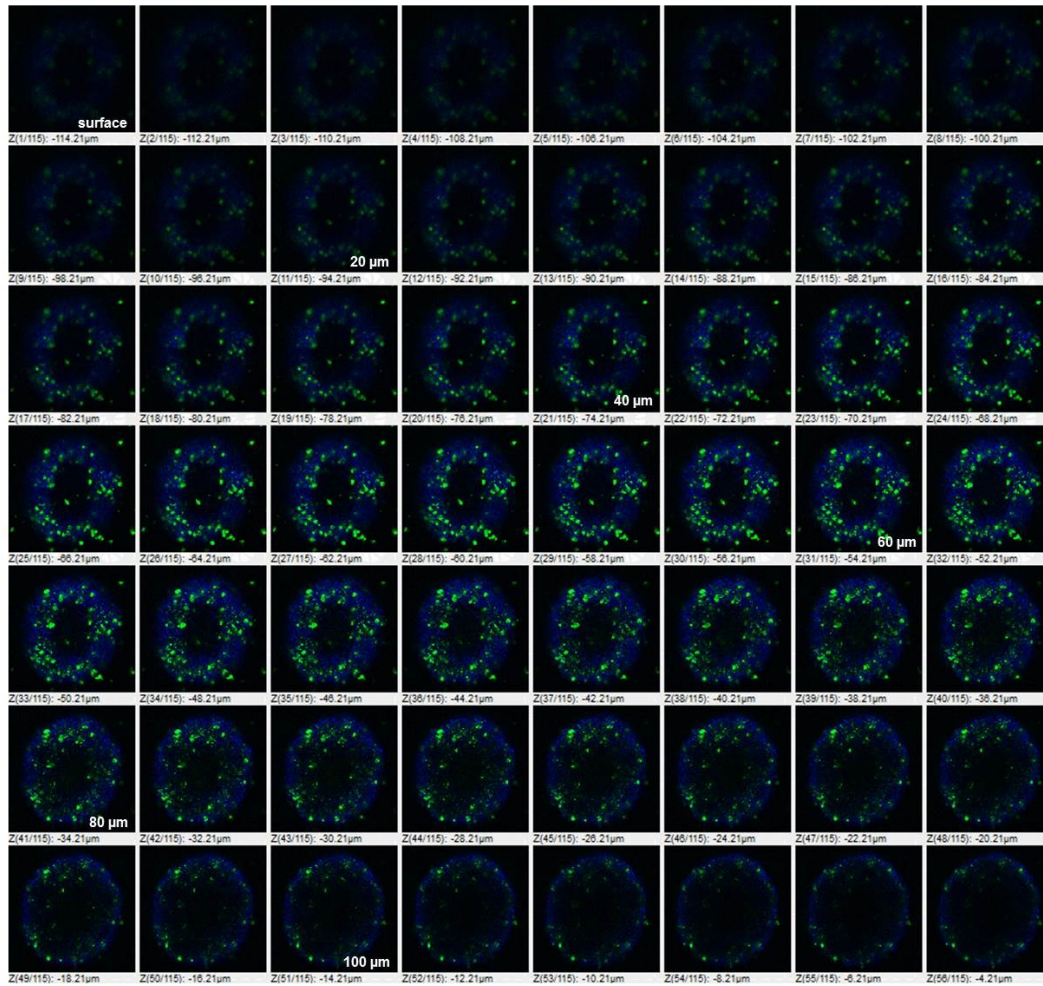
Supplementary figure 3. Gallery display of layer-by-layer scanned images via confocal microscopy showing depth of macrophage penetration in the a) control (untreated), b) nAb-PTX-treated, and c) MSV-nAb-PTX-treated spheroids. The images were scanned with 2 µm increment and macrophages were tagged with DiO to emit green fluorescence and the spheroid was counterstained with DAPI (blue).

b

nAb-PTX



Supplementary figure 3. Gallery display of layer-by-layer scanned images via confocal microscopy showing depth of macrophage penetration in the a) control (untreated), b) nAb-PTX-treated, and c) MSV-nAb-PTX-treated spheroids. The images were scanned with 2 μm increment and macrophages were tagged with DiO to emit green fluorescence and the spheroid was counterstained with DAPI (blue).

c**MSV-nAb-PTX**

Supplementary figure 3. Gallery display of layer-by-layer scanned images via confocal microscopy showing depth of macrophage penetration in the a) control (untreated), b) nAb-PTX-treated, and c) MSV-nAb-PTX-treated spheroids. The images were scanned with 2 µm increment and macrophages were tagged with DiO to emit green fluorescence and the spheroid was counterstained with DAPI (blue).

References

1. A. L. van de Ven, P. Kim, M. Ferrari and S. H. Yun, *Protoc. Exch.*, 2013.
2. H. Jaganathan, J. Gage, F. Leonard, S. Srinivasan, G. R. Souza, B. Dave and B. Godin, *Sci. Rep.*, 2014, **4**, 6468.
3. M. R. Owen and J. A. Sherratt, *IMA J. Math. Appl. Med.*, 1998, **15**, 165-185.
4. M. R. Owen and J. A. Sherratt, *Math. Mod. Meth. Appl. S.*, 1999, **9**, 513-539.
5. H. M. Byrne, S. M. Cox and C. E. Kelly, *Discrete and Continuous Dynamical Systems - Series B*, 2004, **4**, 81-98.
6. M. R. Owen, H. M. Byrne and C. E. Lewis, *Journal of Theoretical Biology*, 2004, **226**, 377-391.
7. S. D. Webb, M. R. Owen, H. M. Byrne, C. Murdoch and C. E. Lewis, *Bull. Math. Biol.*, 2007, **69**, 1747-1776.
8. M. R. Owen, I. J. Stamper, M. Muthana, G. W. Richardson, J. Dobson, C. E. Lewis and H. M. Byrne, *Cancer Res.*, 2011, **71**, 2826-2837.
9. D. Chen, A. A. Bobko, A. C. Gross, R. Evans, C. B. Marsh, V. V. Khramtsov, T. D. Eubank and A. Friedman, *PLoS ONE*, 2014, **9**.
10. P. Macklin, S. McDougall, A. R. A. Anderson, M. A. J. Chaplain, V. Cristini and J. Lowengrub, *J. Math. Biol.*, 2009, **58**, 765-798.
11. S. R. McDougall, A. R. A. Anderson and M. A. J. Chaplain, *J. Theor. Biol.*, 2006, **241**, 564-589.
12. M. Wu, H. B. Frieboes, S. R. McDougall, M. A. J. Chaplain, V. Cristini and J. Lowengrub, *J. Theor. Biol.*, 2013, **320**, 131-151.
13. A. L. van de Ven, M. Wu, J. Lowengrub, S. R. McDougall, M. A. J. Chaplain, V. Cristini, M. Ferrari and H. B. Frieboes, *AIP Advances*, 2012, **2**.
14. *Abraxane® (paclitaxel protein-bound particles for injectable suspension)(albumin-bound)*, Celgene Inc. , 2015.
15. L. J. Nugent and R. K. Jain, *Cancer Res.*, 1984, **44**, 238-244.